Journal of Ethnopharmacology 314 (2023) 116617

Contents lists available at ScienceDirect

Journal of Ethnopharmacology

journal homepage: www.elsevier.com/locate/jethpharm

Cytostatic and cytotoxic effects of a hot water and methanol extract of *Acokanthera oppositifolia* in HepG2 hepatocarcinoma cells

Werner Cordier [a,*], Paul Steenkamp [b], Vanessa Steenkamp [a]

[a] Department of Pharmacology, Faculty of Health Sciences, University of Pretoria, Pretoria, South Africa
[b] Centre for Plant Metabolomics Research, Department of Biochemistry, University of Johannesburg, Auckland Park, South Africa

ARTICLE INFO

Handling Editor: V Kuete

Keywords:
Acokanthera oppositifolia
Apocynaceae
Cytostatic
Cytotoxicity
HepG2
Ouabain

ABSTRACT

Ethnopharmacological relevance: Herb-induced liver injury is poorly described for African herbal remedies, such as *Acokanthera oppositifolia*. Although a commonly used treatment for pain, snake bites and anthrax, it is also a well-known arrow poison, thus toxicity is to be expected.
Aim of the study: The cytotoxicity and preliminary mechanisms of toxicity in HepG2 hepatocarcinoma cells were assessed.
Materials and methods: The effect of hot water and methanol extracts were on cell density, oxidative status, mitochondrial membrane potential, fatty acids, caspase-3/7 activity, adenosine triphosphate levels, cell cycling and viability was assessed. Phytochemicals were tentatively identified using ultra-performance liquid chromatography.
Results: The hot water extract displayed an IC_{50} of 24.26 μg/mL, and reduced proliferation (S- and G2/M-phase arrest) and viability (by 30.71%) as early as 24 h after incubation. The methanol extract had a comparable IC_{50} of 26.16 μg/mL, and arrested cells in the G2/M-phase (by 18.87%) and induced necrosis (by 13.21%). The hot water and methanol extracts depolarised the mitochondrial membrane (up to 0.84- and 0.74-fold), though did not generate reactive oxygen species. The hot water and methanol extracts decreased glutathione (0.42- and 0.62-fold) and adenosine triphosphate (0.08- and 0.26-fold) levels, while fatty acids (2.00- and 4.61-fold) and caspase-3/7 activity (1.98- and 5.82-fold) were increased.
Conclusion: Extracts were both cytostatic and cytotoxic in HepG2 cells. Mitochondrial toxicity was evident and contributed to reducing adenosine triphosphate production and fatty acid accumulation. Altered redox status perturbed proliferation and promoted necrosis. Extracts of *A. oppositifolia* may thus promote necrotic cell death, which poses a risk for inflammatory hepatotoxicity with associated steatosis.

1. Introduction

Traditional remedies form part of the primary healthcare system within Sub-Saharan Africa (James et al., 2018; van Wyk and Prinsloo, 2018) due to its perceived superior efficacy and safety over allopathic medicines, as well as being more cost-effective and aligns to sociocultural beliefs (James et al., 2018; Jing and Teschke, 2018). The use of traditional remedies is often undisclosed to healthcare providers, which complicates diagnosis and treatment due to potential interference with Western medicine (James et al., 2018). *Acokanthera oppositifolia* (Lam.) Codd, a member of the Apocynaceae family, is a small tree with thick leaves, white flowers, and red berries. It is also known as the Bushman's poison as aqueous bark and root decoctions are employed as arrow poison while hunting (Adedapo et al., 2008). Regardless of known toxicity, *A. oppositifolia* is an ethnomedicine for the treatment of pain, snake bites and anthrax (Adedapo et al., 2008). As herbal remedies may be toxic (Amadi and Orisakwe, 2018; James et al., 2018), and their popularity and economic potential are increasing (van Wyk and Prinsloo, 2018), it is necessary to determine the potential detriments to cellular systems. Unfortunately, little research is available regarding the

Abbreviations: ΔΨm, mitochondrial membrane potential; DMSO, dimethyl sulfoxide; ESI, electro spray ionisation; GSH, reduced glutathione; HDMS, high-definition mass spectrometry; PDA, photodiode array; ROS, reactive oxygen species.

* Corresponding author. Department of Pharmacology, Faculty of Health Sciences, School of Medicine, University of Pretoria, Private Bag X323, Arcadia, 0007, Pretoria, South Africa.
E-mail addresses: werner.cordier@up.ac.za (W. Cordier), psteenkamp@uj.ac.za (P. Steenkamp), vanessa.steenkamp@up.ac.za (V. Steenkamp).

https://doi.org/10.1016/j.jep.2023.116617
Received 14 April 2023; Received in revised form 4 May 2023; Accepted 7 May 2023
Available online 13 May 2023
0378-8741/© 2023 The Author(s). Published by Elsevier B.V. This is an open access article under the CC BY-NC-ND license (http://creativecommons.org/licenses/by-nc-nd/4.0/).

efficacy and safety of plants, including those used in Africa (Amadi and Orisakwe, 2018). Thus, activity directed at organs, such as the liver (Amadi and Orisakwe, 2018), is difficult to obtain and little inference can be made about their potential risks.

The liver is necessary for xenobiotic metabolism but is susceptible to direct and indirect toxicity (Amadi and Orisakwe, 2018). Incidences of herb-induced liver injury have increased globally (Amadi and Orisakwe, 2018; Jing and Teschke, 2018), and thus it is important to understand the complex underlying effects thereof. Furthermore, hepatotoxicity testing in preclinical investigation is needed (van Tonder, 2011). Various mechanisms contribute to cytotoxicity, leading to hepatotoxicity. Mitochondrial toxicity is often an underlying mechanism of reactive oxygen species (ROS) generation due to electron leakage (Begriche et al., 2011), with subsequent depletion of endogenous antioxidant (such as reduced glutathione [GSH]) and bolstered oxidative stress (Xu et al., 2004). Mitochondrial alterations may further affect the cell cycle (Kroemer et al., 1998), promote cell death (Kroemer and Reed, 2000), decrease adenosine triphosphate (ATP) production (Pessayre et al., 2012) and/or allow for fatty acid accumulation with induction of hepatosteatosis (Begriche et al., 2011).

Due to the paucity of information on the effects of *A. oppositifolia* on hepatocytes, the study aimed to determine its cytotoxicity and preliminary mechanisms of a hot water (ethomedicinal simulant) and methanol (pharmaceutical relevance) extract in hepatocarcinoma cells.

2. Materials and methods

2.1. Extraction of plant material

Root-bark was collected by Mr Lawrence Tshikudo, and a voucher specimen (LT0019) was stored at the Department of Toxicology (Onderstepoort Veterinary Institute, Pretoria, South Africa). The plant material was cleaned of debris and ground to a fine powder. The hot water extract was made by steeping 10 g root-bark powder in 100 mL boiling distilled water for 15 min. The methanol extract was made by sonicating (40 kHz, 18 °C–20 °C, Bransonic 52, Branson Cleaning Equipment Co.) 10 g root-bark powder in 100 mL methanol for 30 min, agitating the solution for 2 h on an orbital shaker, and extracting for a further 16 h at 4 °C. The methanol extract was decanted, the marc re-extracted thrice, and all supernatants combined.

The extracts were centrifuged (1000 *g*, 5 min) to collect the supernatant, and filtered (0.22 μm). The methanol extract was dried using rotary-evaporation (Büchi Rotovapor R-200, Büchi), and reconstituted in distilled water. The hot water and reconstituted methanol extracts were freeze-dried (Freezone Freeze Dry System, Labconco), and the resultant dry masses dissolved (25 mg/mL) in phosphate-buffered saline (PBS) or dimethyl sulfoxide (DMSO), respectively. The hot water extract was filter-sterilised (0.22 μm) and stored at −80 °C.

2.2. Tentative chemical profiling of extracts

Tentative phytochemical profiling was done using ultra-performance liquid chromatography (UPLC; Waters) coupled in tandem to a photodiode array (PDA; Waters) detector and high-definition mass spectrometer (HDMS; SYNAPT G1, Waters) as described previously by Cordier et al. (2020).

2.3. Cellular maintenance and preparation for seeding

HepG2 (ATCC #HB-8065) cells were cultured in Eagle's Modified Dulbecco's Medium (EMEM) fortified with 10% foetal calf serum (FCS) and 1% penicillin/streptomycin in 75 cm^2 flasks at 37 °C and 5% CO_2. Confluent (90%) cells were sub-cultured using trypsinisation. Detached cells were centrifuged (200 *g* for 5 min) and the pellet resuspended in complete medium. Cells were counted using the trypan blue exclusion assay and diluted with 10% FCS-supplemented medium to 2×10^5 cells/mL or 1.7×10^4 cells/mL for 96- and 24-well plate experiments, respectively.

2.4. Seeding and exposure of cells to crude extracts

2.4.1. 96-Well plate format

A single-plate cytotoxicity method (established by van Tonder [2011]) with modifications described by Cordier et al. (2018) was used to assess the effects of extracts on cell density, oxidative stress (intracellular ROS and GSH), ΔΨm, fatty acid accumulation and caspase-3/7 activity (Sections 2.5.1 to 2.5.6). The effect on lipid peroxidation and ATP levels were assessed separately. To achieve this, two columns were dedicated to each assay allowing for duplicates.

Cells (100 μL) were pipetted into sterile 96-well plates (clear plates for lipid peroxidation (Section 2.6); white plates for all other assays (Sections 2.5.1 to 2.5.6, and Section 2.7). Cells were incubated overnight to facilitate attachment to the plate surface. Attached cells were exposed for 72 h to 100 μL DMSO (0.8%; negative vehicle control), crude extracts (2–200 μg/mL) or the respective positive control prepared in FCS-free medium. The blank consisted of 200 μL 5% FCS-supplemented medium alone to account for sterility and background noise.

2.4.2. 24-Well plate format

For cell cycle analysis, cells were synchronised to the S-phase using the double thymidine blocking method. Two types of media was created; A: 10% FCS-supplemented EMEM; and B: 10% FCS-supplemented EMEM supplemented with 3 mM thymidine (Chiang et al., 2010). Cells were cultured in medium A till confluent, for 16 h in medium B, for 10 h in medium A, and finally for 16 h in medium B. Cells were rinsed with PBS before replacing the medium. Cells were harvested via trypsinisation and prepared for seeding.

For cell cycle (Section 2.8) and cell viability (Section 2.9) analysis, 600 μL synchronised or non-syncrhonised cells were seeded into 24-well plates, and exposed to two-fold the IC_{50} of each extract for 24 and 72 h.

2.5. Single-plate cytotoxicity parameters

For the single-plate cytotoxicity assessment, as described in Section 2.4.1, end-point assays were performed as described in Sections 2.5.1 to 2.5.6.

2.5.1. Cellular density

The sulforhodamine B (SRB) staining assay was used to measure cell density (Vichai and Kirtikara, 2006). Tamoxifen (10 μM in-reaction) was used as positive control. Exposed cells were fixed with 50 μL trichloroacetic acid (50%) overnight at 4 °C. Fixed cells were washed three times under slow-running tap water, and stained with 100 μL SRB (0.057% in 1% acetic acid) for 30 min. Stained cells were washed with 100 μL acetic acid (1%) three times to remove unbound dye. The plates were dried, and the bound dye eluted using 200 μL Tris-buffer (10 mM, pH 7.4). Aliquots (100 μL) were transferred from each well to a clear 96-well plate for spectrophotometric measurement at 510 nm (reference 630 nm) using a Synergy 2 plate reader (Bio-Tek Instruments, Inc.). All the absorbance values were blank-subtracted, and the cell density calculated using the following equation:

$$\text{Cell density (\% relative to negative control)} = \frac{As}{Ac} \times 100$$

where, As = the blank-adjusted absorbance of the sample, and Ac = the blank-adjusted average absorbance of the negative control.

2.5.2. Intracellular reactive oxygen species

The dichloro-dihydrofluorescein diacetate (H_2-DCF-DA) conversion and activation assay was used to measure intracellular ROS (as modified by van Tonder [2011]). Potassium peroxidisulfate (150 μM in-reaction)

was used as positive control. Medium was removed from exposed cells and replaced with 10 μM H_2-DCF-DA for 2 h, after which fluorescence was measured using a FLUOstar Optima plate reader (BMG Labtech) at λ_{ex} = 485 nm and λ_{em} = 520 nm (gain 750). After fluorometric measurement, the cells were fixed as per the SRB assay described in Section 2.5.1. Fluorescence data was blank-subtracted and normalised to cell density. The intracellular ROS was calculated using the following equation:

$$\text{Intracellular ROS (fold} - \text{change relative to negative control)} = \frac{\text{FIs}}{\text{FIc}} \times 100$$

where, FIs = fluorescent intensity of the sample, and FIc = average fluorescent intensity of the negative control.

2.5.3. Intracellular reduced glutathione

The monochlorobimane adduct formation assay was used to measure the intracellular GSH (as modified by Cordier et al. [2013]). n-Ethylmaleimide (10 μM in-reaction) was used as positive control. Medium was removed from exposed cells and replaced with 16 μM monochlorobimane for 2 h. The fluorescence was measured at λ_{ex} = 355 nm and λ_{em} = 460 nm (gain 1250). After fluorometric measurement, the cells were fixed as per the SRB assay described in Section 2.5.1. Fluorescence data was blank-subtracted and normalised to cell density. The intracellular GSH was calculated using the following equation:

$$\text{Intracellular GSH (fold} - \text{change relative to negative control)} = \frac{\text{FIs}}{\text{FIc}} \times 100$$

where, FIs = fluorescent intensity of the sample, and FIc = average fluorescent intensity of the negative control.

2.5.4. Mitochondrial membrane potential

The JC-1 monomer/aggregate ratiometric assay was used to measure ΔΨm (as modified by van Tonder [2011]). Rotenone (100 nM in-reaction) was used as positive control. Medium was removed from exposed cells and replaced with 10 μM JC-1 for 2 h. Fluorescence was measured at λ_{ex} = 492 nm and λ_{em} = 590 nm (gain 1000; for aggregates) and λ_{ex} = 485 nm and λ_{em} = 520 nm (gain 1750; for monomers). The ratio of monomers to aggregates' fluorescence was determined, and ΔΨm calculated using the following equation:

$$\text{m (fold} - \text{change relative to negative control)} = \frac{\text{Rs}}{\text{Rc}} \times 100$$

where, Rs = the ratio of fluorescent intensity of the sample, and Rc = the ratio of average fluorescent intensity of the negative control.

2.5.5. Fatty acid accumulation

The nile red uptake assay was used to measure fatty acid accumulation (Kiela et al., 2005), with oleic acid (200 μM in-reaction) as positive control. Medium was removed from exposed cells and replaced with 10 μM nile red for 2 h. The fluorescence measured at λ_{ex} = 544 nm and λ_{em} = 590 nm (gain 1000). After fluorometric measurement, the cells were fixed as per the SRB assay described in Section 2.5.1. Fluorescence data was blank-subtracted and normalised to cell density. The intracellular fatty acid levels was calculated using the following equation:

$$\text{Intracellular fatty acid levels (fold} - \text{change relative to negative control)} = \frac{\text{FIs}}{\text{FIc}} \times 100$$

where, FIs = fluorescent intensity of the sample, and FIc = average fluorescent intensity of the negative control.

2.5.6. Caspase-3/7 activity

The Ac-DEVD-AMC cleavage assay was used to measure caspase-3/7 activation (as modified by van Tonder [2011]). Staurosporine (10 μM in-reaction) was used as positive control. Plates were centrifuged (200 *g*, 5 min) and the medium was replaced with 25 μL cold lysis buffer for 15 min on ice. After lysis, 100 μL caspase-3/7 substrate buffer (supplemented with 10 μM Ac-DEVD-AMC) was added. Plates were incubated for 4 h at 37 °C, and then for a further 16 h at 4 °C for fixation as per Section 2.5.1. Fluorescence was measured at λ_{ex} = 355 nm and λ_{em} = 460 nm (gain 750). Fluorescence data was blank-subtracted, normalised to the average cell density obtained from Section 2.5.1 and the caspase-3/7 activity calculated using the following equation:

$$\text{Caspase} - 3 \Big/ 7 \text{ activity (fold} - \text{change relative to negative control)} = \frac{\text{FIs}}{\text{FIc}} \times 100$$

where, FIs = fluorescent intensity of the sample, and FIc = average fluorescent intensity of the negative control.

2.6. Lipid peroxidation

The thiobarbituric acid reactive species assay was used to measure lipid peroxidation (as described by Stern et al., 2010). 2,2′-Azobis (2-amidinopropane) dihydrochloride (500 μM in-reaction) was used as positive control. Medium (200 μL) was collected from the exposed cells and replaced with 100 μL trypsin. After 5 min, trypsinised cells (100 μL) were collected and combined with the medium in a 5 mL tube, and vortex-mixed with 100 μL trichloroacetic acid (16.5%) and 100 μL thiobarbituric acid (2.5% in 0.1 M sodium hydroxide and 50 μM ethylenediaminetetraacetic acid). The mixture was heated in a waterbath (95 °C) for 20 min, and 250 μL butanol added. Tubes were vortex-mixed again and allowed to split into an aqueous and organic phase. The organic phase (100 μL) was pipetted into a white 96-well plate and the fluorescence measured at λ_{ex} = 544 nm and λ_{em} = 590 nm (gain 750). Fluorescence data was blank-subtracted, normalised to the average cell density obtained from Section 2.5.1 and the lipid peroxidation activity calculated using the following equation:

$$\text{Lipid peroxidation (fold} - \text{change relative to negative control)} = \frac{\text{FIs}}{\text{FIc}} \times 100$$

where, FIs = fluorescent intensity of the sample, and FIc = average fluorescent intensity of the negative control.

2.7. Adenosine triphosphate levels

The ApoSENSOR™ ATP cell viability chemiluminescence kit was used to measure ATP (as per the manufacturer; MCL Corporation, 2015). Saponin (1% in-reaction) was used as positive control. Medium was removed from exposed cells and replaced with 100 μL nucleotide-releasing buffer. Plates were agitated for 5 min on a shaker to lyse cells. Afterwards, 10 μL ATP-monitoring enzyme was added, and plates read immediately. Luminescence data was blank-subtracted, normalised to the average cell density obtained from Section 2.5.1 and the ATP levels calculated using the following equation:

$$\text{ATP level (fold} - \text{change relative to negative control)} = \frac{\text{LIs}}{\text{LIc}}$$

where, LIs = luminescence intensity of the sample, and LIc = average luminescence intensity of the negative control.

2.8. Cell cycle analysis

Propidium iodide staining was used to assess the effects of the extracts on the cell cycle (Darzynkiewicz and Juan, 1997), with three positive controls: FCS-deprivation (24 h; G0/G1-block), 10 μM methotrexate in-reaction (14 h; G2/M-block) and 20 μM curcumin in-reaction (14 h; S-block). Medium was collected from exposed cells prior to trypsinising them for 5 min. Trypsinised cells were combined with the

collected medium, as well as a 1% FCS-supplemented PBS wash-off to ensure all cells were collected. Cells were centrifuged twice (200*g*, 5 min) with 1% FCS-supplemented PBS. The cells within the combined suspension were fixed with 3 mL cold ethanol (70% [v/v]) overnight at 4 °C. Fixed cells were centrifuged (200 *g*; 5 min) and stained for 40 min at 37 °C with 500 μL propidium iodide staining solution (100 μg/mL RNase, 40 μg/mL prodidium iodide and 0.1% Triton X-100). The DNA distribution was measured flow cytometrically using a FC500 Series flow cytometer (Beckman-Coulter), and analysed using deconvolution software (Multicycle V3.0, WinCycle).

2.9. Cell viability

The Annexin V-FITC/propidium iodide assay was used to measure the effect of extracts on cell viability (Hingorani et al., 2011). Rotenone (50 nM in-reaction; apoptosis) and ethanol-sonication (3 min; necrosis) was used as positive controls. Medium was collected from exposed cells prior to trypsinising them for 5 min. Trypsinised cells were combined with the collected medium, as well as a 1% FCS-supplemented PBS wash-off to ensure all cells were collected. Cells were centrifuged twice (200 *g*, 5 min) with 1% FCS-supplemented PBS, and resuspended in 500 μL Annexin V-binding buffer. Cells were stained for 15 min with 2.5 μL Annexin V-FITC solution. Immediately prior to analysis, 2.5 μL propidium iodide (3 mM) was added as a counterstain. Cellular distribution was measured flow cytometrically using a FC500 Series flow cytometer as FL-1-positive (Annexin V-FITC, early apoptosis), FL-3-positive (propidium iodide, necrosis) or FL-1 and FL-3 positive (late apoptosis, or aponecrosis).

2.10. Statistics

Experiments were conducted with two intra- and three inter-replicates. Results were captured using Microsoft Excel 2010 and analysed with GraphPad Prism 5.0. Results were expressed as the mean ± SEM. The IC_{50} was calculated using non-linear regression. For all plate assays, significant differences relative to the negative control were determined using Kruskal-Wallis with a post-hoc Dunn's test. Flow cytometric results were analysed using two-way analysis of variance (ANOVA) with a post-hoc Bonferroni test. Significance was deemed as $p < 0.05$.

3. Results

The hot water and methanol extracts presented with an extraction yield of 6.1% and 8.1%, respectively. Phytochemicals tentatively profiled within the extracts are presented in Table 1, with representative chromatograms in Fig. 1. More phytochemicals were identified in the hot water extract than the methanol extract.

Positive controls altered biological parameters as expected. Cell density, ΔΨm, GSH and ATP were decreased by 94.2%, 0.34-, 0.85- and 0.99-fold, while ROS, fatty acids, lipid peroxidation and caspase-3/7 activity was increased by 2-, 2.5-, 1.93- and 2.2-fold, respectively. Double thymidine blocking synchronised cells in the S-phase of the cell cycle (71.18%), while positive controls resulted in a G0/G1-block (increase of 8.83%), S-block (increase of 16.69%) and G2/M-block (14.25%). Apoptotic and necrotic controls yielded an increase of 45.94% and 95.10% of cells in each representative quadrant, respectively.

After 72 h exposure to the hot water extract, significant ($p < 0.01$), dose-dependent reduction in cell density was observed at concentrations ≥10 μg/mL, with a maximum decrease of 65.95% (Fig. 2A). The hot water extract displayed a half-maximal inhibitory concentration (IC_{50}) of 24.26 μg/mL. Although the ΔΨm was decreased at all concentrations, it was only significant ($p < 0.01$) at ≥10 μg/mL, with a maximum 0.84-fold reduction at 100 μg/mL (Fig. 2B). Non-significant ($p > 0.05$) reductions in intracellular ROS concentrations were observed (Fig. 2C). Intracellular GSH concentrations were reduced significantly ($p < 0.05$) at concentrations ≥3.2 μg/mL, and plateaued at ≥10 μg/mL (0.56-fold) (Fig. 2D). Although not dose-dependent, fatty acid levels increased significantly ($p < 0.001$) at concentrations ≥10 μg/mL by up to 2.33- and 2.00-fold at 32 μg/mL and 100 μg/mL, respectively (Fig. 2E). Lipid peroxidation remained relatively unaffected apart from a non-significant ($p > 0.05$) increase of 1.24-fold at 3.2 μg/mL (Fig. 2F). The hot water extract reduced ATP levels dose-dependently at all concentrations ($p < 0.05$) between 0.08- to 0.42-fold (Fig. 2G). Although not significant ($p > 0.05$), caspase-3/7 activity was reduced at concentrations ≤3.2 μg/mL (~0.35-fold), but increased at ≥10 μg/mL by up to 1.98-fold (100 μg/mL) (Fig. 2H).

The hot water extract (at the IC_{50}) reduced the percentage of cells in the G0/G1-phase significantly ($p < 0.01$) by 15.10% after 24 h exposure, which reflected as an increase in the number of cells in the sub-G1 (3.03%), S- (5.66%) and G2/M-phase (9.44%) (Fig. 3B). In parallel, cellular viability was decreased by 30.71% ($p < 0.001$) with an increase of necrosis by 29.98% (Fig. 4B). After 72 h exposure, the percentage of cells in the G0/G1-phase decreased by 27.70% ($p < 0.001$), while the percentage of cells in the sub-G1-, S- and G2/M-phase increased by 17.53% ($p < 0.05$), 17.76% ($p < 0.05$) and 10.54%, respectively (Fig. 3E). Viability decreased by 20.83% ($p < 0.01$) with an increase of early apoptosis (2.3%), late apoptosis (1.38%) and necrosis (17.13%; $p < 0.05$) (Fig. 4E).

After 72 h, the methanol extract displayed a calculated IC_{50} of 26.16 μg/mL, with cell density significantly ($p < 0.05$) decreased at concentrations ≥3.2 μg/mL. A maximum reduction of 72.14% at 100 μg/mL was observed (Fig. 5A). A significant ($p < 0.01$) dose-dependent decline in ΔΨm was observed at ≥10 μg/mL, with a maximum change of 0.74-fold at 100 μg/mL (Fig. 5B). The ROS concentrations were reduced at all

Table 1
Phytochemicals tentatively identified within the hot water and methanol extracts of *A. oppositifolia* using ultra-performance liquid chromatography coupled to a photodiode array detector and high-definition mass spectrometer.

Identified phytochemicals	Extract		Empirical formula	MMM (Da)	MCM (Da)	ESI mode
	Hot water	Methanol				
3-Caffeoylquinic acid	X		$C_{16}H_{18}O_9$	354.0951	353.0873	Negative
4-Caffeoylquinic acid	X		$C_{16}H_{18}O_9$	354.0951	353.0873	Negative
5-Caffeoylquinic acid	X		$C_{16}H_{18}O_9$	354.0951	353.0873	Negative
Acobioside A	X	X	$C_{36}H_{56}O_{14}$	712.3670	713.3748	Positive
Acolongifloroside K		X	$C_{29}H_{44}O_{12}$	584.2833	585.2911	Negative and positive
Acovenoside A	X	X	$C_{30}H_{46}O_9$	550.3142	551.3220	Positive
Acovenoside B		X	$C_{32}H_{48}O_{10}$	592.3248	593.3326	Positive
Acovenosigenin (substructure)	X		$C_{23}H_{34}O_5$	390.2406	391.2485	Positive
Opposide		X	$C_{29}H_{44}O_{11}$	568.2884	569.2962	Negative and positive
Ouabagenin (substructure)	X		$C_{23}H_{34}O_8$	438.2254	439.2332	Positive
Ouabain	X	X	$C_{29}H_{44}O_{12}$	584.2833	585.2911	Negative and positive

MMM: Monoisotopic molecular mass; MCM: Monoisotopic calculated mass.

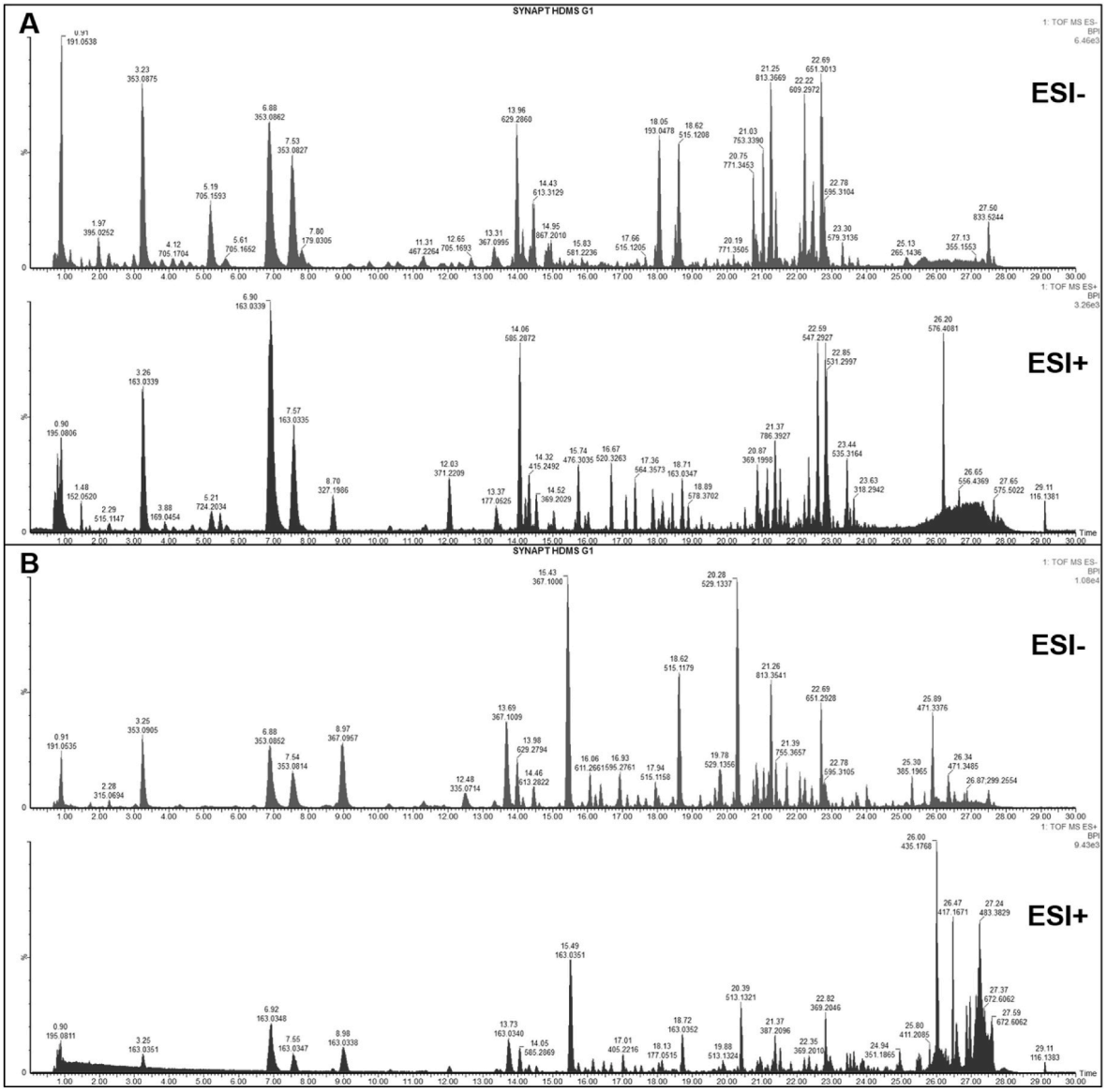

Fig. 1. Chemical profiles of the A) hot water and B) methanol extracts of *A. oppositifolia* as determined by UPLC-HDMS.

concentrations tested, with a significant ($p < 0.05$) decline at ≥32 μg/mL, and complete abolishment at 100 μg/mL (Fig. 5C). Intracellular GSH was significantly ($p < 0.01$) decreased when treated with extract concentrations ranging between 3.2 μg/mL and 32 μg/mL (0.29-fold to 0.43-fold reduction), though increased non-significantly at 100 μg/mL by 1.20-fold (Fig. 5D). Fatty acid levels were significantly ($p < 0.05$) increased at ≥10 μg/mL, and resulted in a 4.61-fold increase at 100 μg/mL (Fig. 5E). Lipid peroxidation was not significantly ($p > 0.05$) altered (Fig. 5F). The ATP levels decreased significantly ($p < 0.05$) by 0.47- and 0.81-fold at all tested concentrations (Fig. 5G). Although caspase-3/7 activity was elevated, significant ($p < 0.05$) changes were only observed at 100 μg/mL by 5.82-fold (Fig. 5H).

After 24 h, the methanol extract decreased the percentage of cells in the G0/G1-phase by 4.90%, while increasing the percentage of cells in the sub-G1- (4.21%), S- (0.70%) and G2/M-phase (4.19%) (Fig. 3C). Cellular viability was reduced by 21.77% ($p < 0.05$), with a parallel increase in early apoptosis (3.08%), late apoptosis (1.19%) and necrosis (17.51%) (Fig. 4C). After 72 h exposure, the number of cells in the G0/G1-phase was further reduced by 20.37% ($p < 0.05$), while the percentage of cells in the sub-G1- (14.69%), S- (1.50%) and G2/M-phase (18.87%; $p < 0.05$) was increased (Fig. 3F). Cellular viability was reduced by 20.53% ($p < 0.01$), and there was an increase of 4.22%, 3.09% and 13.21% of cells in the early apoptotic, late apoptotic and necrotic quadrants, respectively (Fig. 4F).

Although the effect on cell density was similar for both extracts, the hot water extract had a greater effect on cellular processes, especially when cell viability in taken into consideration. Intracellular GSH concentrations, ΔΨm and ATP levels were more prominently reduced by the hot water extract, while the methanol extract increased fatty acid content and caspase-3/7 activity to a greater degree. Although both extracts reduced ROS concentrations, the methanol extract abolished this at higher concentrations. Lipid peroxidation does not appear to occur. The hot water extract increased the percentage of cells in the S- and G2/M-phase, while the methanol extract only increased the cells in the G2/M-phase. Both extracts led to an increase in cells in the sub-G1-phase after 72 h. In parallel, both extracts decreased cellular viability and increased the number of necrotic cells as early as 24 h, however, the hot water extract was more effective in doing so.

4. Discussion

Analyses support the presence of the phytochemicals tentatively

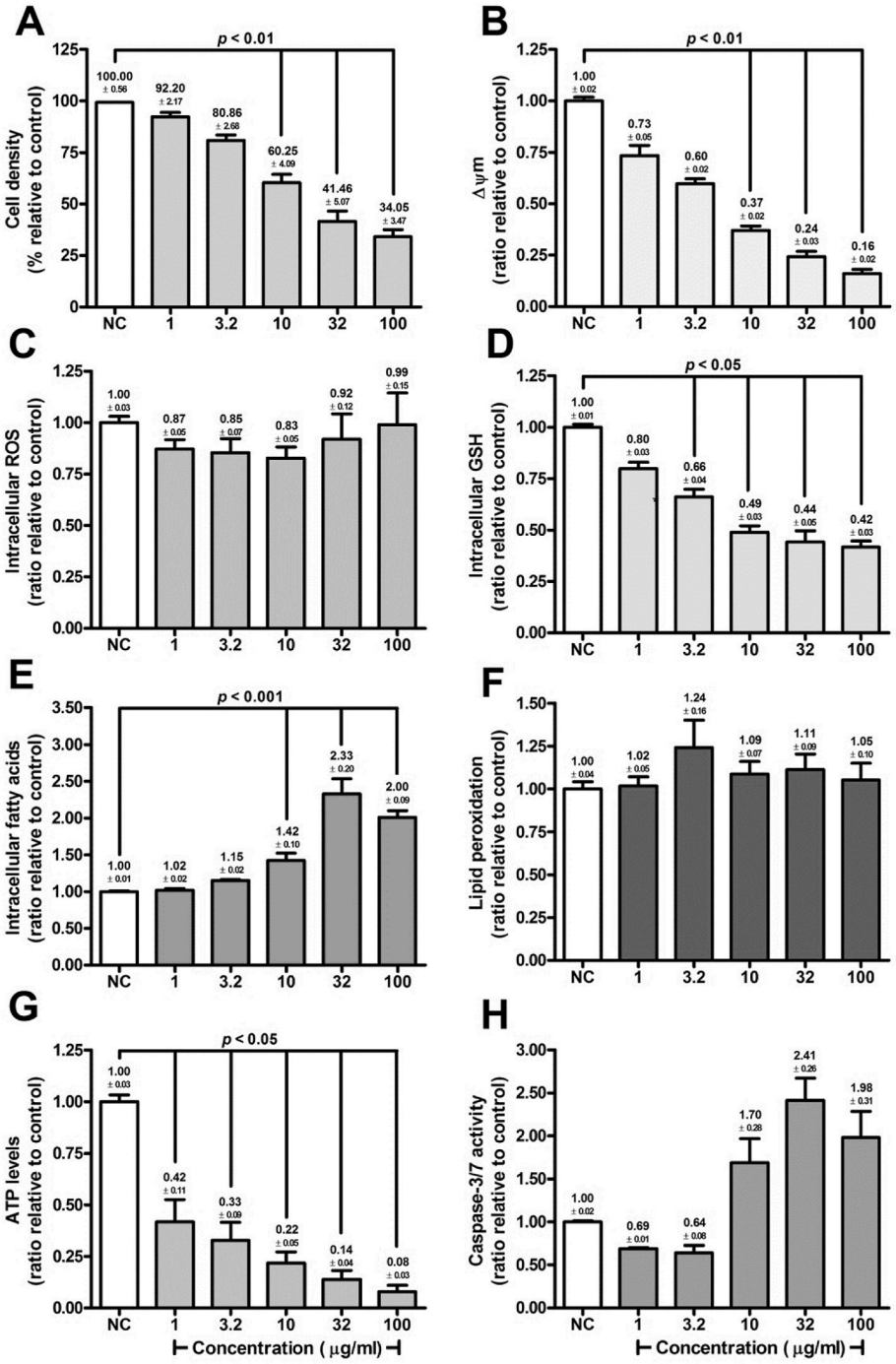

Fig. 2. Alterations to cellular parameters incurred after exposure to the hot water extract of *A. oppositifolia*. A) cell density, B) ΔΨ m, C) ROS concentration, D) GSH concentration, E) fatty acid concentration, F) lipid peroxidation, G) ATP levels and H) caspase-3/7 activity.

identified in the present study (Hauschild-Rogat et al., 1967; Chen, 1970; Ezzat et al., 2016), however, chlorogenic acid (3-*O*-caffeoylquinic acid), crypto-chlorogenic acid (4-*O*-caffeoylquinic acid) and neo-chlorogenic acid (5-*O*-caffeoylquinic acid) have only been reported once before by our research group (Lepule et al., 2019). Given the extraction profiles, ratiometric difference between phytochemicals help explain the similarity and differences in biological effects observed.

Extracts reduced cell density by ~50% at concentrations between 24 and 27 μg/mL, which are considered within the bracket of potentially cytotoxic extracts ($IC_{50} \leq 30$ μg/mL). Lower cytotoxicity has been reported by this group in SH-SY5Y neuroblastoma cells for acetone and methanol root-bark extracts of *A. oppositifolia* (IC_{50} values of 30.5 and 41.4 μg/mL, respectively) (Lepule et al., 2019). Greater cytotoxicity has been described for a methanol leaf extract (human drug-sensitive CCRF-CEM leukaemia [IC_{50} = 2.5 μg/mL] and multi-drug resistant CEM/ADR5000 leukaemia cells [IC_{50} = 2.83 μg/mL]) (Saeed et al., 2016) and dichloromethane root extract (total growth inhibition <12.5 μg/mL in TK10 renal, MCF-7 breast and UACC62 melanoma cell lines) (Fouche et al., 2008). As such, extracts may present cell type-specific cytotoxicity with extraction solvent and plant part affecting their potency. Cytotoxicity data reported for individual phytochemicals suggest acovenoside A, acolongifloriside K, opposide (Kingston and Reichstein, 1974) and ouabain (Gao et al., 2010; Xu et al., 2010a; Ozdemir et al., 2012; Pezzani et al., 2014) as contributors. Ouabain has been reported

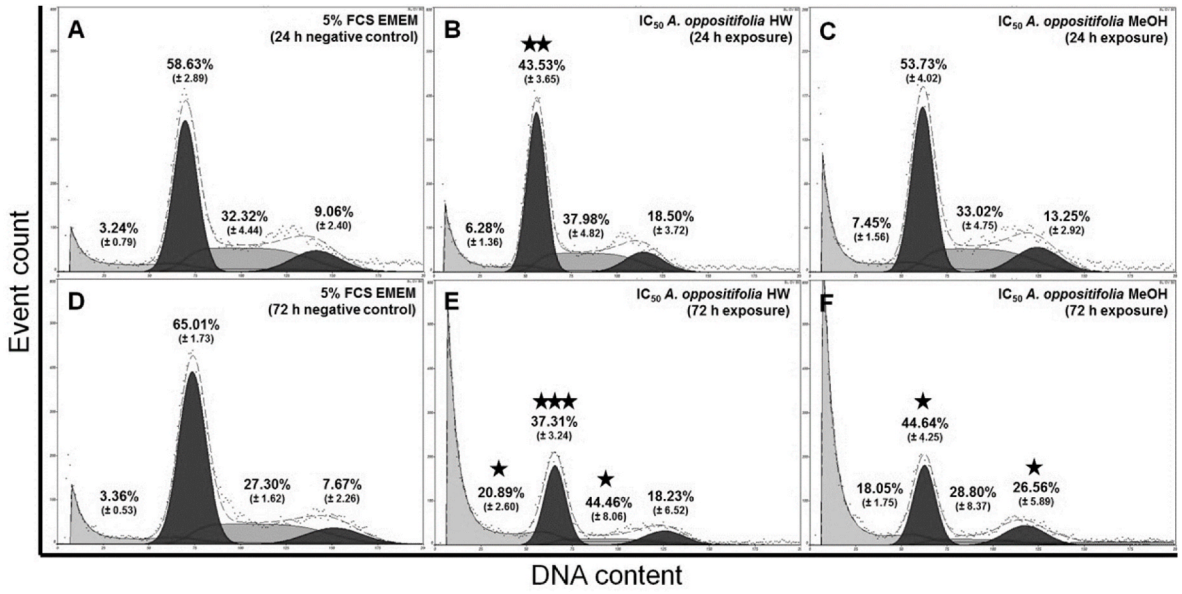

Fig. 3. Alterations to the cell cycle after exposure to the IC_{50} of *A. oppositifolia*; A) negative control (24 h), B) hot water extract (24 h), C) methanol extract (24 h), D) negative control (72 h), E) hot water extract (72 h), F) methanol extract (72 h). Significant difference relative to the respective time points of the negative control: ★ $p < 0.05$, ★★ $p < 0.01$ and ★★★ $p < 0.001$.

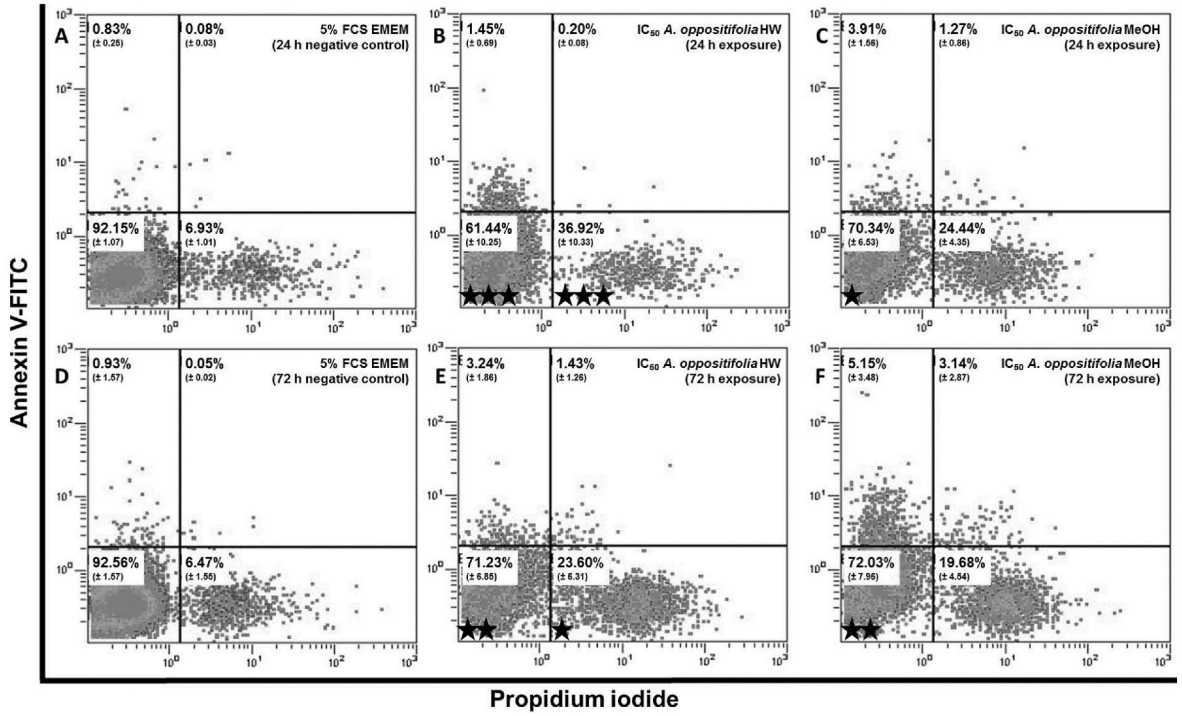

Fig. 4. Alterations to the cell cycle after exposure to the IC_{50} of *A. oppositifolia*; A) negative control (24 h), B) hot water extract (24 h), C) methanol extract (24 h), D) negative control (72 h), E) hot water extract (72 h), F) methanol extract (72 h). Significant difference relative to the respective time points of the negative control: ★ $p < 0.05$, ★★ $p < 0.01$ and ★★★ $p < 0.001$.

to reduce hepatocellular carcinoma cell line viability (Gao et al., 2010; Xu et al., 2010a,b; Ozdemir et al., 2012) and contribute to apoptosis (Song et al., 2020).

Cytostatic and cytotoxic effects decreased cell density as early as 24 h after incubation, with the hot water extract displaying a greater change relative to the negative control. Effects increased over the 72 h exposure time, suggesting time-dependent alterations. Cytostatic effects occurred as a G2/M-arrest, however, the hot water extract also increased cells in the S-phase. Such inhibition is most likely due to DNA damage occurring DNA synthesis (DiPaolo, 2002). In support, the increased percentage of cells in the sub-G1-phase is indicative of DNA fragmentation. Ouabain has been shown to arrest cells in the S- (Gao et al., 2010; Xu et al., 2010a) or G0/G1-phase (Pezzani et al., 2014), as well as incur mitochondrial DNA damage (Nar et al., 2012). Cell viability was reduced after 24 h exposure, highlighting the interplay between cytostatic and cytotoxic effects. It is unclear whether the antiproliferative effect is upstream of the extract-induced necrosis, or rather a parallel process. Necrosis may produce widespread toxicity and downstream

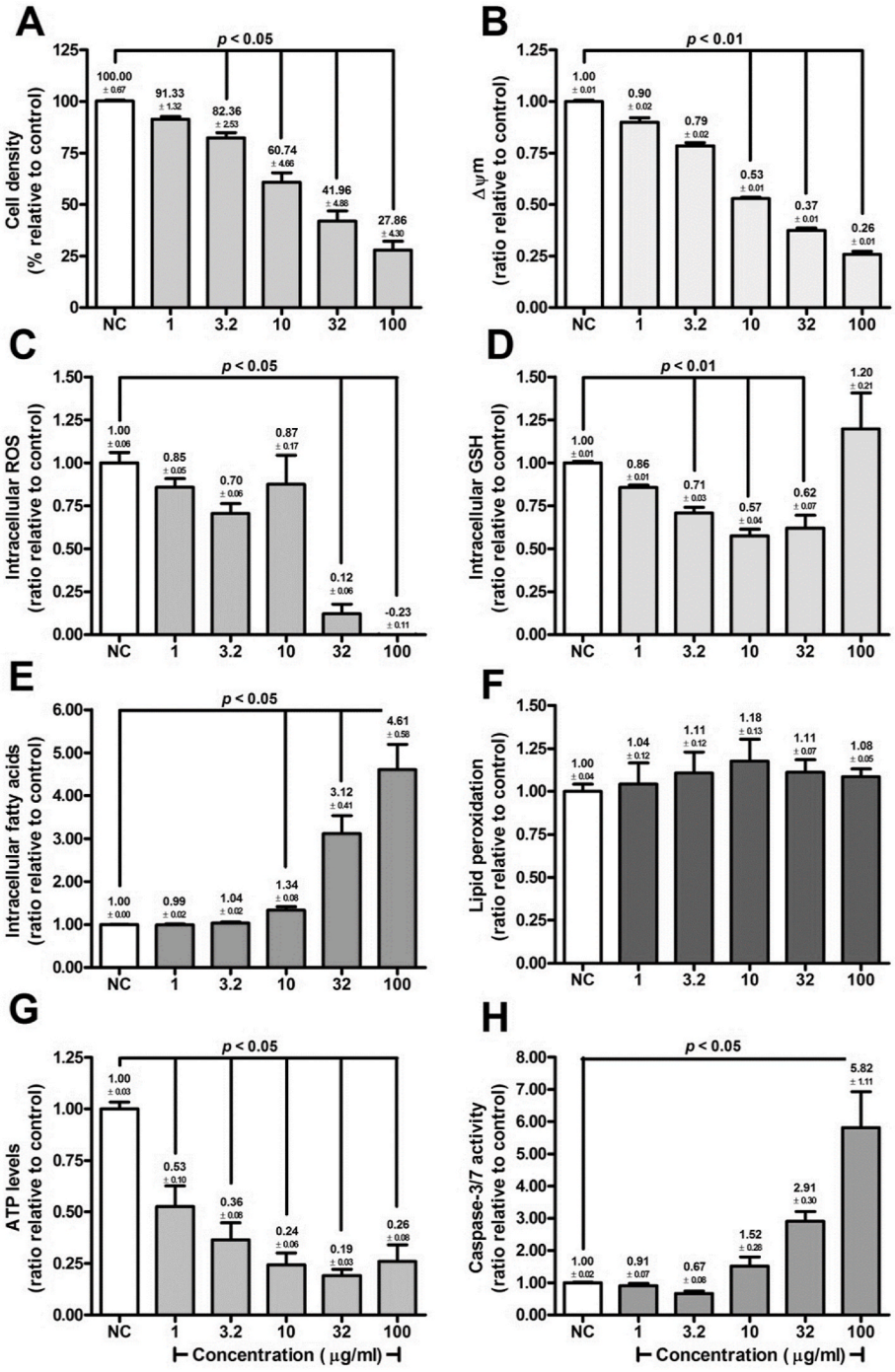

Fig. 5. Alterations to cellular parameters incurred after exposure to the hot water extract of *A. oppositifolia*. A) cell density, B) ΔΨm, C) ROS concentration, D) GSH concentration, E) fatty acid concentration, F) lipid peroxidation, G) ATP levels and H) caspase-3/7 activity.

inflammation (Kroemer et al., 1998), promoting inflammatory hepatotoxicity.

Mitochondrial depolarisation is suggestive of mitochondrial toxicity and appears to be an underlying mechanism to the effects observed. Unwanted opening of the mitochondrial permeability transition pore (MPTP) depolarises the mitochondrial membrane, hindering mitochondrial and cellular function (Kroemer et al., 1998). Contrary to what was expected, the extracts' cytotoxicity were not associated with increased ROS, but rather a decrease. Instead of oxidative stress, the methanol extract appears to have caused reductive stress (Sun et al., 2013), debilitating ROS' function in signaling (Vivancos et al., 2010). Pathways (such as mitogen-activated protein kinases [MAPK]) involved in proliferation, survival and apoptosis, depend on a tightly controlled redox status and mediation by ROS (Vivancos et al., 2010; Son et al., 2011). The time-dependence of this effect on ROS was not assessed though, and thus the initial change to ROS may reflect differently. Ouabain has been shown to down-regulate MAPK1 (Xu et al., 2010a), which supports reductive stress. Compounding the altered redox status, GSH was depleted by both extracts. Although the possibility of early oxidation was not assessed, which may have caused antioxidant depletion, the role of GSH as a phase II conjugate for detoxification (Begriche et al., 2011) cannot be discounted. Excessive GSH depletion may favour hepatocyte necrosis rather than apoptosis (Yuan and Kaplowitz, 2009). The slight elevation in GSH at 100 μg/mL by the methanol extract may

be due to an adaptive *de novo* response (Vivancos et al., 2010). In support of the lack of oxidative stress, lipid peroxidation was not observed.

Depletion of ATP and hindered bioenergetic processes are typically observed following mitochondrial depolarisation (Pessayre et al., 2012). Hindered ATP production occurs due to mitochondrial toxicity, and likely contributed to the G2/M-phase arrest (Gemin et al., 2005). In parallel to the decreased ATP, caspase 3/7 activity was increased, but did not lead to apoptosis. Given the energy-dependent nature of apoptosis (Begriche et al., 2011), the activation suggests an extrinsic pathway was promoted. Surface death receptors activate caspase-8, which in turn directly or indirectly activates caspase-3 (Kroemer and Reed, 2000; Danial and Korsmeyer, 2004). Indirect mechanisms include cleavage of the pro-apoptotic protein Bid or production of ceramide (Kroemer and Reed, 2000; Danial and Korsmeyer, 2004); the latter which is produced from fatty acids (Huang and Freter, 2015). Ceramide is linked to necrosis when mitochondria are damaged, ATP is depleted, or apoptotic pathways are not sufficiently activated (Hetz et al., 2002). Mitochondrial proteins, such as apoptosis-inducing factor, promote cell death and DNA fragmentation in the absence of ATP (Kroemer and Reed, 2000), supporting the increased the percentage of cells in the sub-G1-phase and necrotic quadrant. Ouabain promotes apoptosis (Gao et al., 2010), necrosis (Pezzani et al., 2014) or a mixture thereof (Chen et al., 2014), via ROS generation, calcium influx (Xu et al., 2010b), elevated caspase-3 activity and/or mitochondrial depolarisation (Chen et al., 2014). The contradictory ROS results may be due to variations in the phytochemical matrix between the extracts, thus allowing for interactions between bioactive molecules.

Altered mitochondrial function would activate adenosine monophosphate-activated kinase (AMPK) pathways to promote ATP-production from fatty acids (Pessayre et al., 2012). As ATP levels were reduced, mitochondrial β-oxidation may have been impaired, debilitating fatty acid use and facilitating accumulation (Xu et al., 2004; Bradbury, 2006). Increased fatty acid levels would in turn promote ATP leakage (Brenner et al., 2013), and thus decrease the concentrations thereof as seen in the present study. Given the current profile, hepatosteatosis may occur with extract use.

5. Conclusion

Extracts of *A. oppositifolia* reduced HepG2 viability due to a G2/M-phase cell cycle arrest with associated necrosis, which is linked to underlying mitochondrial dysfunction. Mitochondrial toxicity contributes, and is associated with, reduced GSH and ATP levels, fatty acid accumulation, and stimulation of caspase-3/7 activity. Although redox status was altered, oxidative stress was not observed, but rather reductive stress at 72 h. Given tentative profiling of phytochemicals, ouabain is thought to be the main cytotoxic component, however, interactions between other phytochemicals identified in the extracts cannot be discounted. Given the antiproliferative and necrotic effects, sufficient exposure may present clinically with delayed hepatocellular viability and proliferation, with associated necrosis. As fatty acid accumulation occurred, inflammatory liver disease with hepatosteatotic changes may likely occur. Further studies are warranted to assess the upstream cytotoxicity mechanisms, particularly aligned to proliferative and bioenergetics pathways.

Author contributions

WC and VS co-conceptualised the research project. **WC** conducted all biological assessments, data analysis, and drafted the manuscript. **VS** provided supervision of the project. **PS** conducted chromatographic analyses. **PS and VS** reviewed the manuscript.

Declaration of competing interest

The authors declare that they have no known competing financial interests or personal relationships that could have appeared to influence the work reported in this paper.

Data availability

Data will be made available on request.

Acknowledgements

The authors would like to acknowledge funding support from the National Research Foundation Thuthuka programme (TTK1207112615), as well as technical support from Prof AD Cromarty and Dr JJ van Tonder (Department of Pharmacology, University of Pretoria).

References

Adedapo, A., Jimoh, F., Afolayan, A., Masika, P., 2008. Antioxidant activities and phenolic contents of the methanol extracts of the stems of *Acokanthera oppositifolia* and *Adenia gummifera*. BMC Compl. Alternative Med. 8, 54.

Amadi, C.N., Orisakwe, O.E., 2018. Herb-induced liver injuries in developing nations: an update. Toxics 6, 24.

Begriche, K., Massart, J., Robin, M.-A., Borgne-Sanchez, A., Fromenty, B., 2011. Drug-induced toxicity on mitochondria and lipid metabolism: mechanistic diversity and deleterious consequences for the liver. J. Hepatol. 54, 773–794.

Bradbury, M.W., 2006. Lipid metabolism and liver inflammation. I. Hepatic fatty acid uptake: possible role in steatosis. Am. J. Physiol. Gastrointest. Liver Physiol. 290, G194–G198.

Brenner, C., Galluzzi, L., Keep, O., Kroemer, G., 2013. Decoding cell death signals in liver inflammation. J. Hepatol. 59, 583–594.

Chen, K.K., 1970. Newer cardiac glycosides and aglycones. J. Med. Chem. 13, 1029–1034.

Chen, D., Song, M., Mohamad, O., Yu, S., 2014. Inhibition of Na+/K+-ATPase induces hybrid cell death and enhanced sensitivity to chemotherapy in human glioblastoma cells. BMC Cancer 14, 716.

Chiang, P.-C., Lin, S.-C., Pan, S.-L., Kuo, C.-H., Tsai, I.-L., Kuo, M.-T., Wen, W.C., Chen, P., Guh, J.H., 2010. Antroquinonol displays anticancer potential against human hepatocellular carcinoma cells: a crucial role of AMPK and mTOR pathways. Biochem. Pharmacol. 79, 162–171.

Cordier, W., Gulumian, M., Cromarty, A., Steenkamp, V., 2013. Attenuation of oxidative stress in U937 cells by polyphenolic-rich bark fractions of *Burkea africana* and *Syzygium cordatum*. BMC Compl. Alternative Med. 13, 116–127.

Cordier, W., Steenkamp, P., Steenkamp, V., 2020. Extracts of *Moringa oleifera* lack cytotoxicity and attenuate oleic acid-induced steatosis in an *in vitro* HepG2 model. South Afr. J. Bot. 129, 123–133.

Danial, N.N., Korsmeyer, S.J., 2004. Cell death: critical control points. Cell 116, 205–219.

Darzynkiewicz, Z., Juan, G., 1997. DNA content measurement for DNA ploidy and cell cycle analysis. Curr. Protoc. Cytom. 7, 1–24, 5.

DiPaolo, R., 2002. To arrest or not to G2-M cell-cycle arrest. Clin. Cancer Res. 8, 3512–3519.

Ezzat, S.M., El Gaafary, M., El Sayed, A.M., Sabry, O.M., Ali, Z.Y., Hafner, S., Schmiech, M., Jin, L., Syrovets, T., Simmet, T., 2016. The cardenolide glycoside acovenoside A affords protective activity in doxorubicin-induced cardiotoxicity in mice. J. Pharmacol. Exp. Therapeut. 358, 262–270.

Fouche, G., Cragg, G., Pillay, P., Kolesnikova, N., Maharaj, V., Senabe, J., 2008. *In vitro* anticancer screening of South African plants. J. Ethnopharmacol. 119, 455–461.

Gao, M.-J., Xu, Z., Wang, F., Chen, X., Hu, W., Xu, R., 2010. The linkage between cell cycle S phase arrest and apoptosis on human hepatocellular carcinoma HepG2 induced by Na+, K+-ATPase inhibitors via regulating proteins associated with cell cycle. Chin. Pharmacol. Bull. 26, 452–456.

Gemin, A., Sweet, S., Preston, T.J., Singh, G., 2005. Regulation of the cell cycle in response to inhibition of mitochondrial generated energy. Biochem. Biophys. Res. Commun. 332, 1122–1132.

Hauschild-Rogat, P., Weiss, E., Reichstein, T., 1967. Die cardenolide von *Acokanthera oppositifolia* (Lam.) Codd. 3. Mitteilung. Isolierung weitere Cardenolide und teilweise Strukturaufklärung. Glykoside und Aglykone, 301. Mitt. Helv. Chim. Acta. 50, 2299–2321.

Hetz, C.A., Hunn, M., Rojas, P., Torres, V., Leyton, L., Quest, A.F., 2002. Caspase-dependent initiation of apoptosis and necrosis by the Fas receptor in lymphoid cells: onset of necrosis is associated with delayed ceramide increase. J. Cell Sci. 115, 4671–4683.

Hingorani, R., Deng, J., Elia, J., Mcintyre, C., Mittar, D., 2011. Detection of Apoptosis Using the BD Annexin V FITC Assay on the BD FACSVerseTM System. Application Note, BD Biosciences.

Huang, C., Freter, C., 2015. Lipid metabolism, apoptosis and cancer therapy. Int. J. Mol. Sci. 16, 924–949.

James, P.B., Wardle, J., Steel, A., Adams, J., 2018. Traditional, complementary and alternative medicine use in Sub-Saharan Africa: a systematic review. BMJ Glob. Health 3, e000895.

Jing, J., Teschke, R., 2018. Traditional Chinese medicine and herb-induced liver injury: comparison with drug-induced liver injury. J. Clin. Transl. Hepatol. 6, 57–68.
Kiela, P.R., Midura, A.J., Kuscuoglu, N., Jolad, S.D., Sólyom, A.M., Besselsen, D.G., Timmermann, B.N., Ghishan, F.K., 2005. Effects of *Boswellia serrata* in mouse models of chemically induced colitis. Am. J. Physiol. Gastrointest. Liver Physiol. 288, G798–808.
Kingston, D., Reichstein, T., 1974. Cytotoxic cardenolides from *Acokanthera longiflora* Stapf. and related species. J. Pharmaceut. Sci. 63, 462–464.
Kroemer, G., Reed, J.C., 2000. Mitochondrial control of cell death. Nat. Med. 6, 513–519.
Kroemer, G., Dallaporta, B., Resche-Rigon, M., 1998. The mitochondrial death/life regulator in apoptosis and necrosis. Annu. Rev. Physiol. 60, 619–642.
Lepule, K.H., Cordier, W., Steenkamp, P., Nell, M., Steenkamp, V., 2019. The ability of three African herbal remedies to offer protection against an *in vitro* model of Parkinson's disease. South Afr. J. Bot. 126, 121–131.
MCL Corporation, 2015. ApoSENSOR ATP Cell Viability.
Nar, R., Bedir, A., Alacam, H., Kilinc, V., Avci, B., Salis, O., Gulten, S., 2012. Tumour. Biol. 33, 2107–2115.
Ozdemir, T., Nar, R., Kilinc, V., Alacam, H., Salis, O., Duzgun, A., Gulten, S., Bedir, A., 2012. Ouabain targets the unfolded protein response for selective killing of HepG2 cells during glucose deprivation. Cancer Biother. Radiopharm. 27, 457–463.
Pessayre, D., Fromenty, B., Berson, A., Robin, M.-A., Lettéron, P., Moreau, R., Mansouri, A., 2012. Central role of mitochondria in drug-induced liver injury. Drug Metab. Rev. 44, 34–87.
Pezzani, R., Rubin, B., Redaelli, M., Radu, C., Barollo, S., Cicala, M.V., Salvà, M., Mian, C., Mucignat-Caretta, C., Simioni, P., Iacobone, M., Mantero, F., 2014. The antiproliferative effects of ouabain and everolimus on adrenocortical tumor cells. Endocr. J. 61, 41–53.
Saeed, M.E.M., Meyer, M., Hussein, A., Efferth, T., 2016. Cytotoxicity of South-African medicinal plants towards sensitive and multidrug-resistant cancer cells. J. Ethnopharmacol. 186, 209–223.
Son, Y., Cheong, Y., Kim, N., Chung, H., Kang, D.G., Pae, H., 2011. Mitogen-activated protein kinases and reactive oxygen species: how can ROS activate MAPK pathways. J. Signal. Transduct., 792639, 2011.
Song, Y., Lee, S.-Y., Kim, S., Choi, I., Kim, S.-H., Shum, D., Heo, J., Kim, A., Kim, K.M., Seo, H.R., 2020. Inhibitors of Na^+/K^+ ATPase exhibit antitumor effects on multicellular tumor spheroids of hepatocellular carcinoma. Sci. Rep. 10, 5318.
Stern, S.T., Potter, T.P., Neun, B., 2010. NCL method GTA-4: Hep G2 hepatocyte lipid peroxidation assay. Nanotechnol. Character. Lab. https://doi.org/10.17917/H65D-SJ70. https://ncl.cancer.gov/resources/assay-cascade-protocols.
Sun, C., Zhang, H., Ma, X.F., Zhou, X., Gan, L., Liu, Y.Y., Wang, Z.H., 2013. Isoliquiritigenin enhances radiosensitivity of HepG2 cells via disturbance of redox status. Cell Biochem. Biophys. 65, 433–444.
van Tonder, J., 2011. Development of an *In Vitro* Mechanistic Toxicity Screening Model using Cultured Hepatocytes. University of Pretoria. Thesis.
van Wyk, A.S., Prinsloo, G., 2018. Medicinal plant harvesting, sustainability and cultivation in South Africa. Biol. Conserv. 227, 335–342.
Vichai, V., Kirtikara, K., 2006. Sulforhodamine B colorimetric assay for cytotoxicity screening. Nat. Protoc. 1, 1112–1116.
Vivancos, P., Wolff, T., Markovic, J., Pallardó, F., Foyer, C., 2010. A nuclear glutathione cycle within the cell cycle. Biochem. J. 431, 169–178.
Xu, J., Diaz, D., O'Brien, P., 2004. Applications of cytotoxicity assays and pre-lethal mechanistic assays for assessment of human hepatotoxicity potential. Chem. Biol. Interact. 150, 115–128.
Xu, Z., Wang, F., Xu, R., Hu, W., Chen, X., 2010a. Effect of Na(+)/K(+)-ATPase alpha1 siRNA and ouabain upon cell cycle in human hepatoma HepG2 cell and its mechanism. Zhonghua Yixue Zazhi 90, 813–817.
Xu, Z.-W., Wang, F.-M., Gao, M.-J., Chen, X.-Y., Hu, W.-L., Xu, R.-C., 2010b. Targeting the Na+/K+-ATPase alpha1 subunit of hepatoma HepG2 cell line to induce apoptosis and cell cycle arresting. Biol. Pharm. Bull. 33, 743–751.
Yuan, L., Kaplowitz, N., 2009. Glutathione in liver diseases and hepatotoxicity. Mol. Aspect. Med. 30, 29–41.